Journal of Materials Chemistry A

PAPER

View Article Online
View Journal | View Issue

Cite this: J. Mater. Chem. A, 2016, 4, 9293

Direct observation of reversible oxygen anion redox reaction in Li-rich manganese oxide, Li_2MnO_3, studied by soft X-ray absorption spectroscopy†

Masatsugu Oishi,*[a] Keisuke Yamanaka,[b] Iwao Watanabe,[ab] Keiji Shimoda,[a] Toshiyuki Matsunaga,[a] Hajime Arai,[a] Yoshio Ukyo,[a] Yoshiharu Uchimoto,[c] Zempachi Ogumi[a] and Toshiaki Ohta[b]

Received 7th January 2016
Accepted 14th May 2016

DOI: 10.1039/c6ta00174b

www.rsc.org/MaterialsA

Li-rich layered oxides have attracted attention as promising positive electrode materials for next-generation lithium-ion secondary batteries because of their high energy storage capacity. The participation of the oxygen anion has been hypothesized to contribute to these oxides' high capacity. In the present study, we used O K-edge and Mn L-edge X-ray absorption spectroscopy (XAS) to study the reversible redox reactions that occur in single-phase Li-rich layered manganese oxide, Li_2MnO_3. We semiquantitatively analyzed the oxygen and manganese reactions by dividing the charge/discharge voltage region into two parts. The O K-edge XAS indicated that the electrons at the oxygen site reversibly contributed to the charge compensation throughout the charge/discharge processes at operating voltages between 2.0 and 4.8 V *vs.* Li^+/Li^0. The Mn L-edge XAS spectra indicated that the Mn redox reaction occurred only in the lower-voltage region. Thus, at higher potentials, the electrons, mainly at the oxygen site, contributed to the charge compensation. Peaks whose energies were similar to peroxide appeared in and then disappeared from the O K-edge spectra obtained during the reversible redox cycles. These results indicate that the reorganization of the oxygen network in the crystal structure affects the redox components. By using two kinds of detection modes with different probing depths in XAS measurements, it was found that these redox reactions are bulk phenomena in the electrode.

1. Introduction

A series of Li-rich layered oxide systems, Li_2MnO_3–$LiMO_2$ (M = Ni, Co, and Mn), have gained attention as high-capacity positive electrodes for lithium-ion secondary batteries (LIBs), which exhibit a reversible capacity of *ca.* 250 mA h g^{-1} or higher.[1–5] This capacity is approximately twice that of conventional positive LIB electrode materials such as $LiCoO_2$;[6,7] thus, Li-rich layered oxides have attracted significant interest as high-capacity electrode materials for next-generation LIBs. Researchers have hypothesized that not only the transition-metal cations but also the oxygen anions contribute to the reversible charge compensation reactions.[8–14] We have investigated the charge compensation mechanism of $Li_{1.16}Ni_{0.15}Co_{0.19}Mn_{0.50}O_2$ using both hard and soft X-ray absorption spectroscopy (XAS).[11,15] The Ni and Co K- and L-edge XAS spectra indicated that Ni and Co ions reversibly participated in the charge compensation, whereas the Mn K- and L-edge XAS indicated that the Mn ions remained in the tetravalent state. The O K-edge XAS spectra changed in accordance with charge and discharge during the reversible cycles, suggesting that the reversible redox reaction of oxygen anions, in addition to those of Ni and Co cations, contributed to the high capacity of $Li_{1.16}Ni_{0.15}Co_{0.19}Mn_{0.50}O_2$. The $Li_{1.16}Ni_{0.15}Co_{0.19}Mn_{0.50}O_2$ electrode exhibited a reversible charge/discharge capacity of *ca.* 240 mA h g^{-1}, corresponding to the extraction/insertion of nearly 0.78 mol of Li^+ during the reversible cycles. When considering the redox reactions of Ni^{2+}/Ni^{4+} and Co^{3+}/Co^{4+}, which correspond to 0.49 mol of Li^+ in total, the expected capacity for the $Li_{1.16}Ni_{0.15}Co_{0.19}Mn_{0.50}O_2$ electrode material is 150 mA h g^{-1}. This capacity is smaller than the experimentally observed reversible capacity. The difference between the theoretical and observed capacities is 90 mA h g^{-1} (0.29 mol of Li^+), which must originate from the redox reaction of oxygen.

The Li-rich layered oxide is a mixture system composed of Li-rich layered manganese oxide, Li_2MnO_3, and a conventional layered oxide, $LiMO_2$. Its reversible capacity exceeds that of the conventional layered oxides. The Li_2MnO_3 phase in the composite system plays an essential role in the realization of the

[a]Office of Society-Academia Collaboration for Innovation, Kyoto University, Gokasho, Uji, Kyoto 611-0011, Japan. E-mail: m-ooishi@kyoto-u.ac.jp; Fax: +81-774-38-4996; Tel: +81-774-38-4940

[b]SR Center, Ritsumeikan University, Kusatsu, Shiga 525-8577, Japan

[c]Graduate School of Human and Environmental Studies, Kyoto University, Yoshida-Honmachi, Sakyo-ku, Kyoto 606-8501, Japan

† Electronic supplementary information (ESI) available. See DOI: 10.1039/c6ta00174b

reversible high capacity. Thackeray *et al.*[3] reported that the Li_2MnO_3 component acts as a stabilizing unit in the electrode structure, which enables high practical capacities. Li_2MnO_3 was considered to be electrochemically inactive because the Mn^{4+} in the structure is not further oxidized to compensate for the extraction of Li ions during the charge process.[14,16] Surprisingly, however, the Li_2MnO_3 electrode functions alone as a positive electrode in an LIB. Yu *et al.*[17] reported that Li_2MnO_3 is electrochemically active, exhibiting a discharge capacity of ~260 mA h g^{-1} at 25 °C. Several mechanisms have been proposed to solve this puzzle, including mechanisms that involve electron extraction from the oxygen 2p level,[18–20] the removal of oxygen atoms,[2,17,21] or the replacement of Li^+ with H^+, which is the oxidation product of the electrolyte.[21–24] The structural variation of Li_2MnO_3 upon Li^+ extraction and insertion has recently been intensively studied to elucidate the phase transformation that occurs in this material.[20,25–27] Whereas structural changes during the delithiation/lithiation reactions have been elucidated in many of these reports, none included direct experimental evidence that explains the mechanism of the large reversible capacity.

Here, we focus on the electronic structure variation of the Li_2MnO_3 electrode during the extraction/insertion reactions of Li^+ ions. The participation of oxygen ions in the charge compensation reactions in the Li_2MnO_3 electrode has mainly been discussed theoretically in previous reports[18–20] because direct observation of the redox reaction of oxygen is difficult. In terms of the charge balance, the high capacity of Li_2MnO_3 cannot be explained by the cation redox reactions alone. Under such a situation, the oxygen–anion redox reaction is well recognized in the Li-rich layered oxide system. However, the details of the redox reaction mechanism of oxygen anions during reversible cycling have not been elucidated. Sathiya *et al.*[14] directly observed an oxygen–anion redox reaction for a $Li_2Ru_{1-x}Sn_xO_3$ solid solution system by using X-ray photoelectron spectroscopy (XPS) and electron paramagnetic resonance to demonstrate the reversible contributions of anionic species. The direct observation of oxygen in Li_2MnO_3 is limited to an XPS study reported by Han *et al.*[28] Since XPS is a surface-sensitive method with a detection depth of several nanometers or less, the behavior of oxygen anions in the bulk electrode is unclear. To discuss the relationship between the charge compensation mechanism and the capacity of the electrode, detailed knowledge is needed concerning the redox reactions occurring in the electrode bulk. In this paper, soft XAS was used to study the electronic structure of oxygen and manganese in Li_2MnO_3. Bulk and surface XAS spectra were obtained simultaneously using two different detection modes: a fluorescence yield (FY) and a total electron yield (TEY) mode. The former is bulk sensitive with a detection depth of approximately 500 nm, whereas the latter is surface sensitive, with a detection depth less than 10 nm from the sample surface.[11,29] Mn L-edge and O K-edge XAS spectra over the near-edge region are associated with the electronic transitions from the corresponding core levels to the hybridized orbitals of Mn 3d and O 2p near the Fermi level of Li_2MnO_3. Therefore, the degree of oxygen redox contribution to the charge compensation could be directly evaluated by the soft XAS technique. XAS measurements were carried out for the Li_2MnO_3 electrodes in different states of charge to elucidate the redox potentials of manganese and oxygen in Li_2MnO_3 during the charge/discharge processes.

2. Experimental

2.1 Sample preparation

Pulverized Li_2MnO_3 was prepared by solid-state reaction of $LiOH \cdot H_2O$ (High Purity Chemicals, 99%) and $MnCO_3$ (High Purity Chemicals, 99.9%). The powder of each starting compound was carefully weighed at an appropriate ratio of Li : Mn = 2 : 1 and mixed together using a ball mill. The mixed powder was calcined at 973 K for 24 h in air. Structural characterization was performed by powder XRD (Smartlab, Rigaku Co.) equipped with a Cu-Kα radiation source operated at 40 kV and 40 mA. The XRD analysis confirmed that the Li_2MnO_3 powder synthesized was single phase with *C*2/*m* space symmetry and was free of any obvious impurity phase (Fig. S1†).[30,31] The SEM images of the powder are shown in Fig. S2.† The powder was composed of primary particles with a size of *ca.* 100 nm; these primary particles were aggregated into secondary particles of micron size.

The cathode electrode was fabricated from mixtures composed of the active material (80%), carbon (10%), and PVdF binder (10%). The electrolyte used was 1 M $LiPF_6$ in ethylene carbonate/dimethyl carbonate (1 : 2 ratio by volume). A coin cell (Hosen Co.) was used for the electrochemical evaluation. The cell consisted of the cathode electrode and a lithium metal anode, which were separated by a porous polypropylene film. The charge and discharge current density was 10 mA g^{-1}, with a cutoff voltage of 2.0 to 4.8 V *vs.* Li^+/Li^0; the cell was operated at 298 K. Fig. 1 shows the charge and discharge profiles of the Li_2MnO_3 electrode. The characteristic charge profile of the Li-rich layered oxides with a voltage plateau was observed during the initial charge, followed by an irreversible discharge capacity. After the irreversible initial cycle, the charge and discharge reactions were quite reversible, with no voltage plateau. The samples for the XAS measurements were electrochemically prepared at several SOCs during the initial irreversible cycle and reversible 2nd and 5th cycles, as numbered in Fig. 1. In the reversible cycles, the d*Q*/d*V* plot exhibited three distinct regions: a clear redox couple at *ca.* 3.0 V *vs.* Li^+/Li^0 and two weak redox couples at higher potentials. To confirm the reversibility in the XAS character after the 2nd cycle, samples were also prepared for the 5th 4.8 V charged and 2.0 V discharged states. After the specified charge/discharge processes, the cells were disassembled in an argon-filled glove box. The cathode materials were removed from the cells, rinsed with dimethyl carbonate to remove the electrolyte, and dried. The parameters of the XAS samples are listed in Table S1.†

2.2 X-ray absorption spectroscopy measurements

The Mn L- and O K-edge XAS spectra were collected at the soft X-ray beam line, BL-11, at the SR Center, Ritsumeikan University (Shiga, Japan). To prevent the samples from being exposed

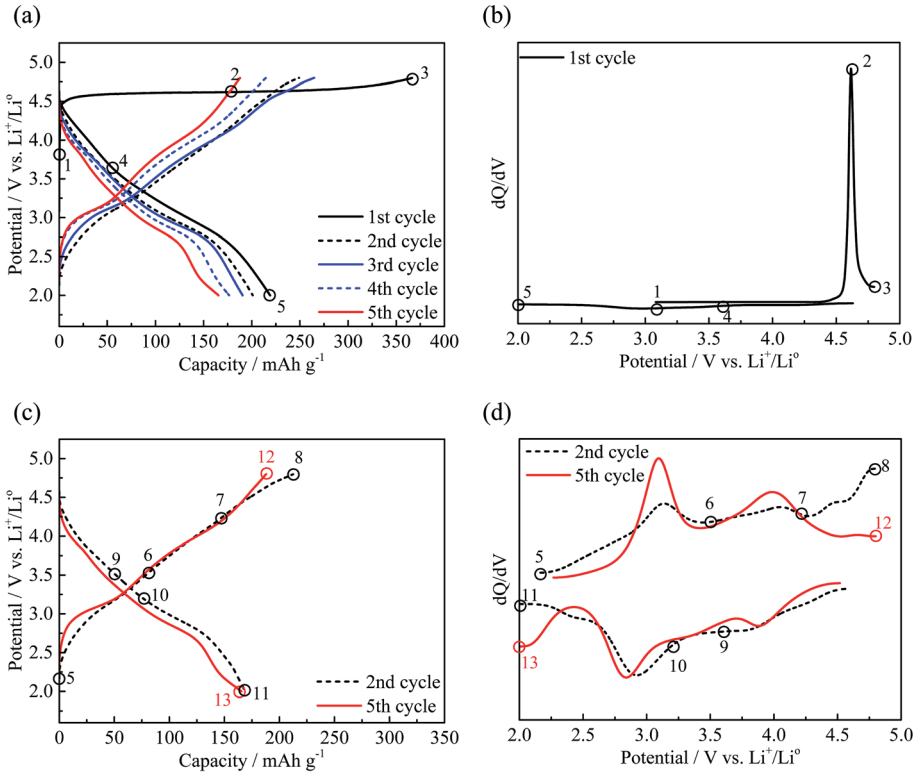

Fig. 1 (a) Charge/discharge profiles for Li_2MnO_3 electrodes. The XAS sample numbers are given for only the first cycle for clarity. (b) dQ/dV plot for the first cycle sample. (c) Sample numbers are given for the 2nd and 5th cycle samples. (d) dQ/dV plots for the 2nd and 5th cycle samples.

to air, the electrode samples were transferred to the high-vacuum sample chamber of BL-11 using a transfer vessel filled with argon gas.[32] The XAS spectra were simultaneously obtained in both the total electron yield (TEY) mode using a sample drain current and the partial fluorescence X-ray yield (PFY) mode using a silicon drift detector (KETEK, VITUS R100 with a 0.1 μm thick Parylene-N film window). For the Mn L-edge PFY XAS, inverse partial fluorescence yield (IPFY) spectra were collected, in which the inverse of the fluorescence yield in the O K-edge region was used as the Mn L-edge fluorescence intensity to suppress the self-absorption effect,[33] which might have distorted the Mn PFY spectra reported previously.

3. Results

3.1 XAS spectra during the reversible charge/discharge cycles

As shown in Fig. 1(a), the reaction that occurs during the 1st charging process differs substantially from those of the 1st discharge and subsequent cycles. Because the most important aim of this research is to elucidate the reactions that occur during the reversible charge/discharge processes, we start by describing the 2nd and succeeding cycles.

Fig. 2 shows the Mn $L_{II,III}$-edge XAS spectra collected during the 2nd (a) charge and (b) discharge in the TEY and PFY modes. The Mn $L_{II,III}$-edge spectra of MnO, Mn_2O_3, and MnO_2 are also shown for reference. The Mn L_{III}-edge spectrum changes substantially depending on the oxidation state. The Mn L_{II}-edge band shifts to higher photon energy with increasing oxidation state. The spectra for the 1st (spectrum no. 5) and 2nd (spectrum no. 11) discharged states are regarded as a mixture of those for MnO (640.1 eV), Mn_2O_3 (641.6 eV), and MnO_2, indicating that the Mn ions exist as Mn^{2+} and Mn^{3+} states in addition to Mn^{4+}. A strong Mn^{2+} peak was observed in the TEY-mode spectrum, indicating that the Mn ions are reduced to a greater extent at the electrode surface than in the bulk at the discharged state. When the electrode was charged to 3.5 V (no. 6), the spectrum appeared to be that of MnO_2, indicating that most of the Mn ions were oxidized to Mn^{4+}. Further charging to 4.2 (no. 7) and 4.8 V (no. 8) yielded only small differences in the TEY mode (at the surface) and almost no difference in the PFY mode (in the bulk). These results indicate that the valence state of Mn ions remained unchanged at charging potentials above 3.5 V. Discharge is the opposite process to that of charge. Upon discharge from 4.8 (no. 8) to 3.2 V (no. 10), the spectra in Fig. 2(b) remained unchanged, especially those in the bulk; however, upon further discharge from 3.2 (no. 10) to 2.0 V (no. 11), they changed substantially, especially at the surface. In summary, the valence state of Mn ions remained unchanged during charge/discharge processes between 3.6 and 4.8 V but steeply oxidized/reduced between 2.0 and 3.6 V.

Fig. 3 shows the O K-edge XAS spectra obtained in the TEY and PFY modes during the 2nd (a) charge and (b) discharge. Each spectrum is composed of two characteristic profiles: a pre-edge region below 534 eV and a broad band above 534 eV. The broad band above 534 eV corresponds to the transition from O

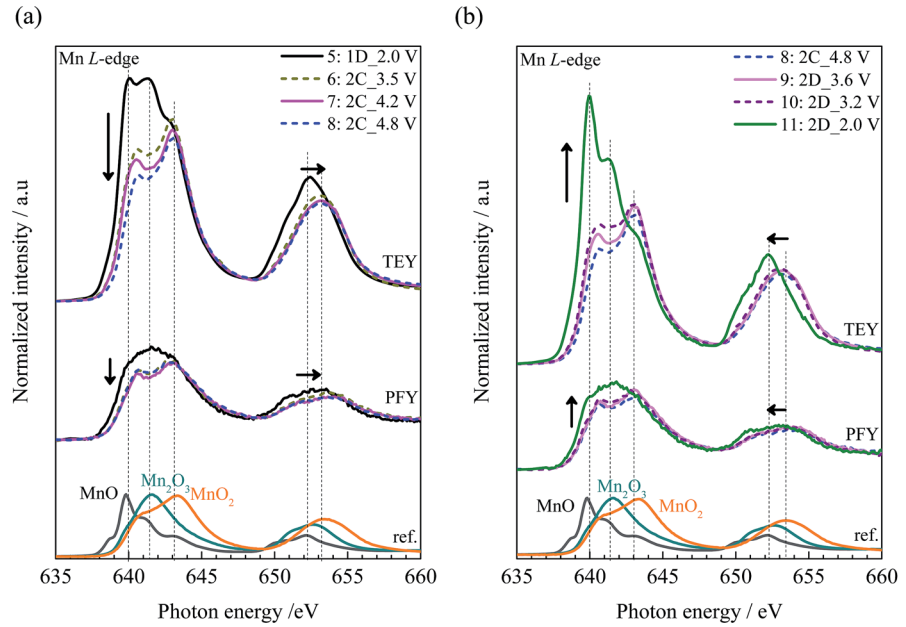

Fig. 2 Mn $L_{II,III}$-edge XAS spectra for Li_2MnO_3 electrodes; the spectra were obtained during (a) charging and (b) discharging processes in the 2nd cycle. Included are the spectra for MnO, Mn_2O_3, and MnO_2 as reference spectra for Mn^{2+}, Mn^{3+}, and Mn^{4+} ions, respectively.

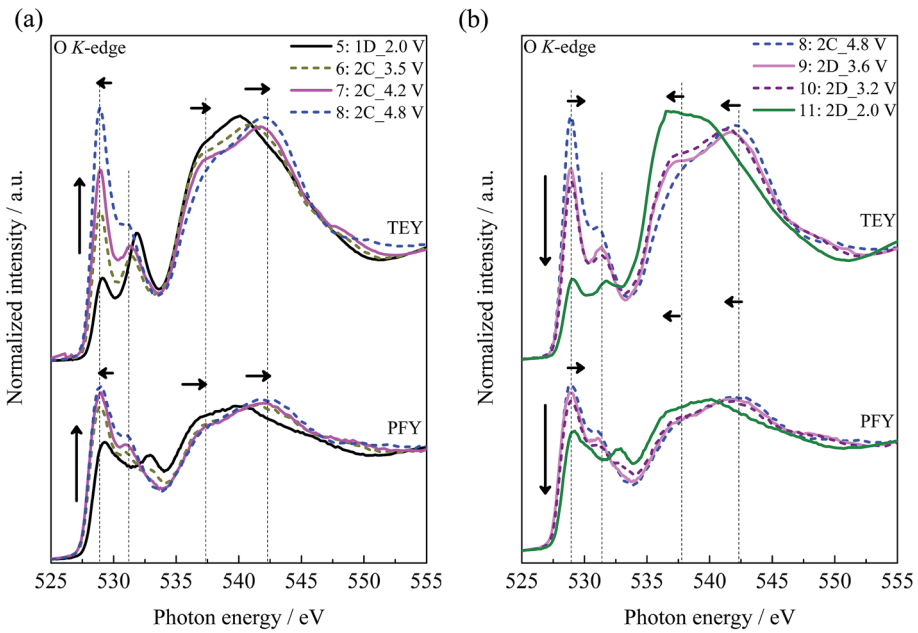

Fig. 3 O K-edge XAS spectra for Li_2MnO_3 electrodes obtained during (a) charging and (b) discharging processes in the 2nd cycle.

1s to the hybridized states of Mn 4sp and O 2p orbitals, Mn_{4sp}–O_{2p}. This transition is associated with the transition to the antibonding σ* states,[34] whose energy shifts sensitively with the metal–ligand bond distance.[35,36] The pre-edge structure corresponds to the transition to hybridized states of Mn 3d and O 2p orbitals, Mn_{3d}–O_{2p},[29,37,38] which consists of an intense peak at 528.9 eV and a sub-peak at 531 eV.

In the charging process, the broad band above 534 eV shifted to higher energy until 3.5 V and remained almost unchanged afterwards to 4.8 V in both the TEY and PFY modes. During the discharging process, the broad band remained mostly unchanged from 4.8 V to 3.2 V and shifted to lower energy from 3.2 V to 2.0 V. The upward shift is associated with the shortening of the metal–oxygen bond distance. Therefore, the spectral behavior indicates that the ionic radius of the Mn ion decreased after its oxidation during charging. Upon the reverse reaction of discharge, the band shifted to lower energy, corresponding to the reduction of the Mn ions. In addition, the

position of a pre-edge peak at approximately 529 eV shifted to lower energy by approximately 0.2 eV upon charging from 2.0 V to 3.5 V and did not move after 3.5 V (to show these details, the O K-edge XAS spectra over the pre-edge region are expanded in Fig. S4(a) and (b)† for the charge and discharge processes, respectively).

In the reverse discharge process, the pre-edge peak remained unchanged from 4.8 V until 3.2 V and shifted to higher energy afterwards until 2.0 V. In addition, the shift of the pre-edge peak in energy reflects the change in the valence state of Mn ions because the energy is closely related to the effective charge of the coordinating metal ion.[39] The shifts to lower and higher energies correspond to the oxidation and reduction of Mn ions, respectively. The aforementioned conclusion derived from the O K-edge XAS results is consistent with the findings from the present Mn L-edge XAS data. Specifically, the Mn ions were oxidized during charging from 2 V to 3.5 V and remained unchanged afterwards and, during the reverse discharge process, the Mn ions remained unchanged from 4.8 V to 3.2 V and were reduced afterwards.

The intensity of the pre-edge peaks in the O K-edge spectra increased and decreased upon charge and discharge, respectively. These intensity changes also indicate the participation of oxygen during the charge/discharge processes. Generally, the intensity of the O K pre-edge structure is strongly related to the metal 3d states.[38] In the Li_2MnO_3 structure, the Mn 3d orbitals are hybridized with the O 2p orbitals. The increase in the pre-edge intensity thus indicates the creation of hole states at the Mn_{3d}–O_{2p} level by the charging process. The pre-edge intensity increased throughout the operating voltage range between 2.0 V and 4.8 V during charge and decreased during discharge. In contrast, the Mn L-edge XAS spectra remained unchanged over the higher voltage region above 3.5 V. This result implies that the electrons are extracted from the Mn_{3d}–O_{2p} hybridized orbitals below 3.5 V, whereas those in the higher-voltage region are mainly extracted from the O 2p orbitals.

To ensure the experimental findings concerning the reversible reactions, the results from the 5th cycle are also presented in Fig. S3.† The spectra taken during the 5th cycle are similar to those of the 2nd cycle, suggesting that the same charge compensation mechanism occurred after the 2nd cycle until the 5th cycle.

3.2 XAS spectrum change during the initial charge and discharge

As already mentioned, the reactions occurring during the first charge process differ substantially from those of the following processes. The first charge is the activation process of the cathode material, and its structure after the activation might be quite different from that of the pristine state.

Fig. 4 shows the Mn $L_{II,III}$-edge XAS spectra collected during the initial charge. The spectra before the charge are similar to those of MnO_2, with a main peak at 643.1 eV and a sub-peak at 640.7 eV caused by the spin multiplicity and the crystal field effect, and a L_{II}-edge peak at 653.4 eV. These spectra clearly show that the valence state of the Mn in the Li_2MnO_3 electrode

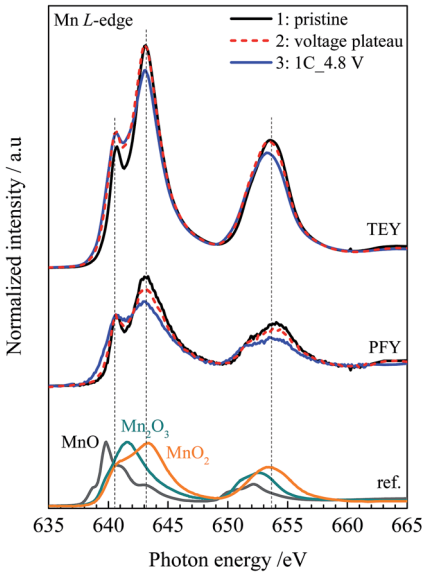

Fig. 4 Mn $L_{II,III}$-edge XAS spectra for Li_2MnO_3 electrodes obtained during the first charging process. The spectra for MnO, Mn_2O_3, and MnO_2 are included as reference spectra for Mn^{2+}, Mn^{3+}, and Mn^{4+} ions, respectively.

is 4+. During the initial charge, neither the TEY- nor the PFY-mode spectra showed clear changes such as those observed during the reversible charge/discharge cycles. During the charging process, the L_{III}-edge spectra exhibited a decrease in the main peak intensity and an increase in the sub-peak intensity. The L_{II}-edge peak shifted to a lower photon energy. These changes of the Mn L-edge spectra indicate that some of the Mn ions were reduced during the initial charging process. Notably, during the initial charge, the Mn ions did not participate in the charge compensation reaction, which must be accompanied by the extraction of Li^+ ions.

Fig. 5 shows the O K-edge XAS spectra taken during the initial charge. Each spectrum is composed of pre-edge peaks and a broad band starting from 534 eV. The energies of pre-edge peaks remained unchanged during the initial charge. The broad band structures in both the TEY- and PFY-mode spectra revealed no clear trends during the initial charge. Meanwhile, the pre-edge peak area increased gradually with increasing charge (the O K pre-edge structure is expanded in Fig. S5†). The increase in the pre-edge area indicates the creation of hole states at the Mn_{3d}–O_{2p} level. In the initial charge, the Mn L-edge XAS spectrum indicated that the valence state of Mn was mostly unchanged or slightly reduced. If the Mn ions are reduced, electrons must be inserted into the Mn_{3d}–O_{2p} level, leading to the reduction in the hole concentration at the Mn_{3d}–O_{2p} level. However, the experimental results showed an increase in the pre-edge area, suggesting an increase in the hole concentration. This result is opposite to that expected on the basis of the valence change of Mn ions. Therefore, we presume that the increase in the O K- pre-edge area during the charging process indicates the reorganization of new oxygen networks formed in addition to Mn_{3d}–O_{2p} bands upon charge. The details will be given in the Discussion section.

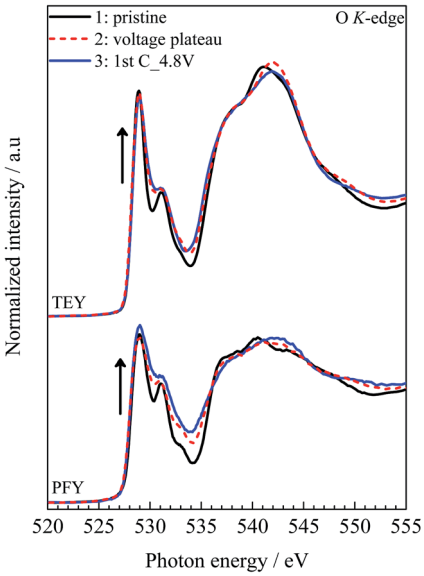

Fig. 5 O K-edge XAS spectra during the initial charging process for Li_2MnO_3 electrodes.

4. Discussion

4.1 Overall charge compensation mechanism of the Li_2MnO_3 electrode

The relative amount of Mn^{2+}, Mn^{3+} and Mn^{4+} at each stage can be roughly estimated by fitting the experimental XAS data with those of MnO (Mn^{2+}), Mn_2O_3 (Mn^{3+}), and the pristine sample (Mn^{4+}). The results of the fitting analysis are given in Fig. 6. The numbered points correspond to the samples indicated in Fig. 1. The results for the 1st charged state (no. 3) and those obtained during the reversible cycles afterwards are given for (a) the bulk samples (PFY) and for (b) the surface samples (TEY). In the bulk, the relative amount of Mn^{2+} does not change during the charge/discharge processes. The Mn species participating in the reversible redox reactions are Mn^{3+} and Mn^{4+} over the potential region of 2 V to 3.6 V. In the region of 3.6 V to 4.8 V, their contents were mostly unchanged, or it seemed that the Mn^{4+} content rather decreased and that of the Mn^{3+} increased with charge and *vice versa* with discharge. The reduction of a part of Mn by charging is queer, however, was also recognized from the hard XAS analysis as given in Fig. S6.† The Mn K-edge spectra shifted to higher photon energy by charging from 2.0 V (no. 5) to 3.5 V (no. 6), and further charging above 3.5 V induced a slight shift to lower energy. These results for the reversible processes are essentially consistent with the present Mn L-edge XAS behavior.

During the first charging process both the TEY and PFY data given in Fig. 6(c) and (d) indicated substantial reduction of Mn at the last stage (from no. 2 to 3). The corresponding K-edge spectra given in Fig. S6(a)† also indicated the reduction of Mn at the higher potential region (from no. 2 to 3). Since the K-edge spectrum change must be in part due to the structural rearrangements taking place in the initial charge process, the evaluation of the valence states from the hard X-ray XAS is difficult.[40]

Since the charging process is an oxidation process, the reduction of Mn ions by charge is quite interesting. Similar phenomena have been discussed. Tarascan's group[14,41,42] suggested the reduction of the transition metals in the Li-rich layered oxides by charge. They discussed the oxidation of anions that accompanies a reduction of Ru ions in the charging process in Li-rich Li_2RuO_3 materials and they named it as the reductive coupling mechanism. Ohzuku *et al.*[43] mentioned the possible reduction of the transition metal in the charging process of lithium nickel manganese oxides when electrons are removed from oxygen ions causing the rearrangement of the electrons of anions and cations. Our results indicated that electrons are mainly extracted from the O 2p orbitals in the higher-voltage region, which caused the rearrangement of electrons in the Mn_{3d}–O_{2p} level of Li_2MnO_3 that resulted in the partial reduction of Mn.

In contrast, at the surface (Fig. 6(b)), the Mn^{2+} ion already exists at the 1st charged state (no. 3), and its relative amount increases with the redox cycles. After several cycles, almost all Mn ions at the surface are in the 2+ state at the discharged state. Precisely describing the Mn redox reaction at the surface is difficult because surface XAS is sensitive to various experimental conditions. However, during the reversible cycles, the Mn^{3+} ions apparently do not participate in the reaction; in the lower-voltage region, the Mn^{2+}/Mn^{4+} couple participates, and in the higher voltage region, almost no Mn ions participate. Because the electrons exchanged between Mn^{2+} and Mn^{4+} are double the amount exchanged between Mn^{3+} and Mn^{4+}, the present finding predicts that the battery capacity originating from the Mn-ion redox reaction can be enhanced through effective utilization of the surface region of the electrode. Taminato *et al.*[44] reported that they obtained a higher capacity by using a thinner Li_2MnO_3 film electrode compared to a thicker one; this result is consistent with our findings.

We observed that, during the reversible cycles, the Mn redox reactions proceeded mainly over the lower-potential range between 2.0 V and 3.6 V. In contrast, the O K-edge XAS structure changed throughout the potential range between 2.0 V and 4.8 V. At potentials greater than 3.6 V, the O K-edge spectrum changed, whereas the Mn L-edge spectrum did not. These results are schematically represented in Fig. 7. Thus, at higher potentials, the electrons in the oxygen site mainly contributed to the charge compensation for the extraction/insertion of Li^+ ions. When the density of states for Li_2MnO_3 over the Fermi level region are considered, the energy level of the Mn^{3+}/Mn^{4+} redox couple is located above the top of the O 2p band, whereas the Mn^{4+}/Mn^{5+} redox couple is located far below the top of the O 2p band. During charge, the electron extraction primarily occurs *via* the Mn^{3+}/Mn^{4+} redox couple at approximately 3.0 V, where a peak is observed in the dQ/dV plot in Fig. 1(d). Upon further charging to potentials above the Mn^{3+}/Mn^{4+} level, the electrons are consequently extracted from the top of the O 2p band. The valence state of the Mn ions does not exceed 4+ because the Mn^{4+}/Mn^{5+} redox couple is located so far below the top of the O 2p level that, even in a higher-voltage region, the holes are created mostly in the O 2p orbitals.

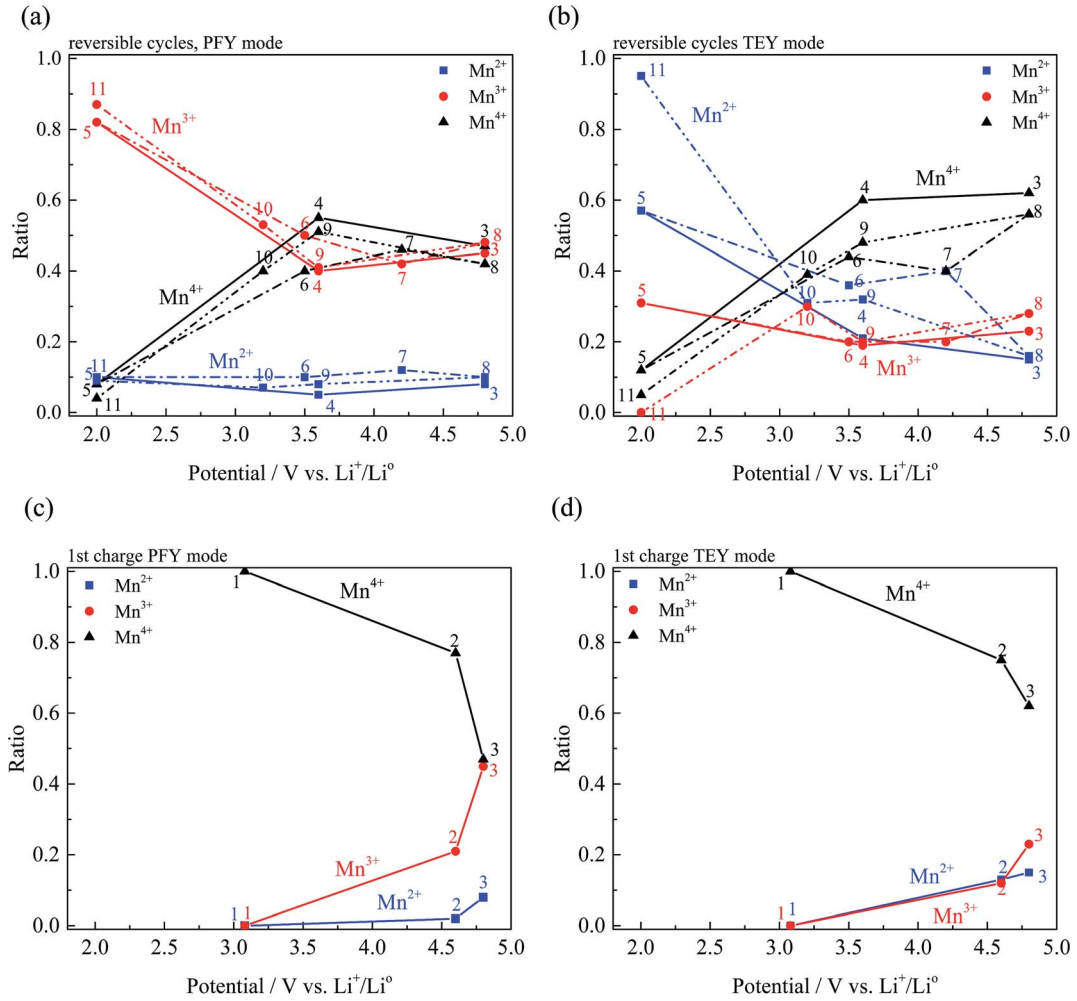

Fig. 6 The changes in the relative amount of Mn^{2+}, Mn^{3+} and Mn^{4+} states during the charge and discharge processes. Their ratios were calculated by fitting the Mn L_{III} pre-edge spectra with those for MnO, Mn_2O_3, and pristine samples as representing Mn^{2+}, Mn^{3+}, and Mn^{4+} states, respectively. (a) The results from the PFY data for the 1st discharge and the following cycles and (b) from the TEY data. (c) and (d) are the results obtained for the initial charge (activation process) in PFY (bulk sensitive) and TEY (surface sensitive) modes, respectively. The numbered points correspond to the samples indicated in Fig. 1.

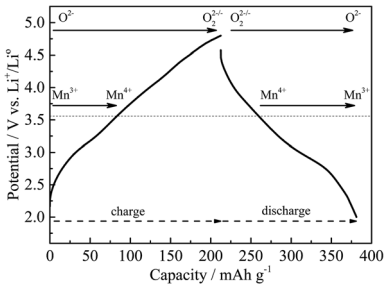

Fig. 7 Suggested redox reactions occurring during the reversible charge/discharge processes.

We studied the changes in the O K-edge XAS spectra in greater detail by extracting the difference spectra, which are displayed in Fig. 8. We first focus on the initial charging process (Fig. 8(a)). During the initial charge, the charge induced by the extraction of Li^+ ions is compensated solely by the oxidation of oxygen. The line 2–1 in Fig. 8(a) indicates the spectrum of the pristine sample (no. 1) subtracted from that with an approximately 40% charge (no. 2) and the line 3–1 indicates that of the fully charged (no. 3) sample subtracted from no. 1. Two distinct peaks, P1 and P2, appear at the lower- and higher-energy sides, respectively, of the main pre-edge peak at 529.0 eV (in Fig. 5). The energy of P1 at approximately 528 eV coincides well with that of KO_2 reported by Kang *et al.*,[45] whereas the peak P2 at approximately 530 eV is located near that of Li_2O_2 reported by Yilmaz *et al.*[46] The superoxide has an empty π^* level, leading to the appearance of a peak at 528 eV. The peroxide has an empty σ^* level, causing a broad peak at approximately 530 eV. The appearance of P1 and P2 peaks indicates the formation of the peroxide and superoxide ionic-like states during the 1st charge. In the TEY mode, a negative peak Q1 at 528.5 eV is recognized, indicating the reduction of the hole states in the Mn_{3d}–O_{2p} band. If the charging reaction extracts electrons from the metal 3d band, holes should be created in this state, leading to an

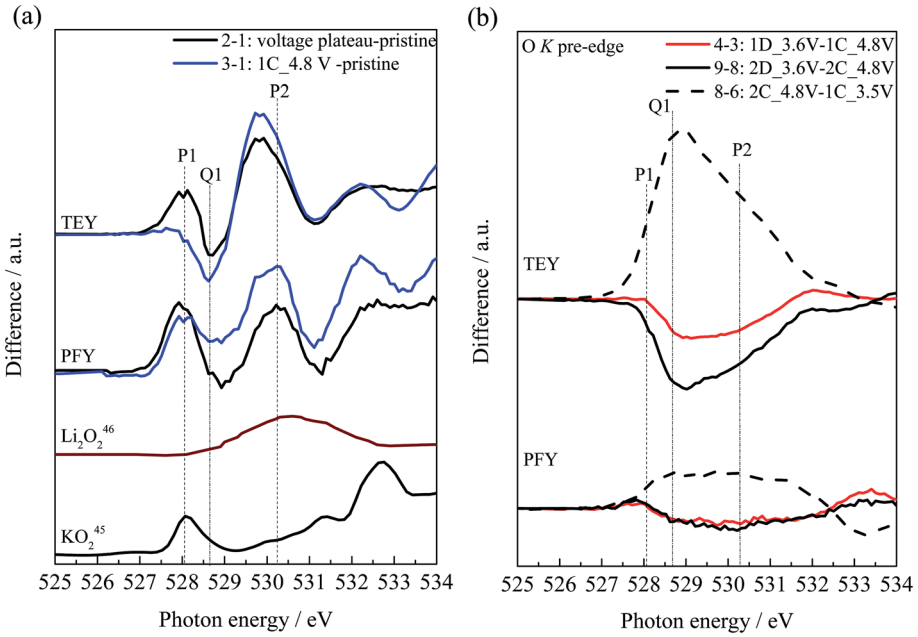

Fig. 8 (a) The difference spectra of O K-edge XAS results in the initial charge process for the Li_2MnO_3 electrodes. The line 2–1 indicates the difference spectra between the spectrum of the pristine state (spectrum no. 1) and that of the voltage plateau state (spectrum no. 2), and the line 3–1 indicates the difference spectra between that of the pristine state (spectrum no. 1) and that of 4.8 V charged states (spectrum no. 3). Included are the reference spectra for KO_2 reported by Kang *et al.*[45] and Li_2O_2 reported by Yilmaz *et al.*[46] (b) The difference spectra of O K-edge XAS results in the reversible cycles over higher potential regions where the Mn valence states follow little the SOC. The lines 4–3 and 9–8 are for the 1st and 2nd discharge processes between 3.6 V and 4.8 V, and 8–6 for the 2nd charge process between 3.5 V and 4.8 V, respectively.

enhancement of Q1 intensity. In the present case, by contrast, Mn ions were reduced during charge, the density of holes decreased, and the negative Q1 peak then appeared in the difference spectra of the electrode surface.

The difference spectra obtained for the reversible cycles are depicted in Fig. 8(b). The difference spectra were calculated for the higher potential region (3.6–4.8 V) where the redox reaction mainly occurs at the oxygen ions. In the difference spectra, a band structure over the 528–532 eV region appears positively during charge and negatively during discharge, and the spectral profiles are merely mirror images of each other. The broad peak located around 530 eV looks similar in energy and shape to that of Li_2O_2.[45] Thus, the peroxide-like component must be one of the reversible redox components.

The difference spectra from the reversible cycles (Fig. 8(b)) are not the same as those of the 1st charge (Fig. 8(a)). These results reflect the fact that the pristine sample changes its structure irreversibly by the activation process, *i.e.*, the 1st charge. Oxygen loss has been reported by Yu *et al.*,[17] and others.[2,21] The formation of Mn^{3+} in the initial charge insists this fact. Moreover, the difference spectra for the 2nd cycle also indicate that the reversible redox reactions and the environment around oxygen at the surface are somewhat different from those in the bulk. The peak energy of 528.5 eV in the TEY spectra is most similar to the energy of peak Q1 related to the hole state in the Mn_{3d}–O_{2p} orbitals created by the valence change of Mn ions. The appearance of the strong peak at 528.5 eV in the TEY-mode spectra at high potential ranges indicates that the redox reaction of the Mn ions also occurs at the electrode surface. This is consistent with the TEY results given in Fig. 6(b) indicating the participation of Mn ions at the surface, while its participation is small at the bulk (Fig. 6(a)).

4.2 The redox reaction of oxygen anions

Density functional theory calculations for Li_2MnO_3 predicted that its top valence band is predominantly contributed by oxygen orbitals.[18–20] Therefore, the electron extraction in the charging process occurs from the oxygen orbitals and, with increasing SOC, the density of empty oxygen orbitals increases. The oxygen orbitals then condense to form empty oxygen bands. Goodenough and Kim[47,48] reported that the oxidation of the metal oxide at high voltages would result in the creation of holes in anion p-bands and that these anion p-holes condense into dianion p–p antibonding states. This energetic scheme was discussed in detail by Rouxel for some of the transition metal chalcogenides[49] and later by Sathiya *et al.*[14] In the delithiation reaction of Li_2MnO_3, we have observed that the condensation of the anion p-holes was recognized as the chemical forms of O_2^{2-}/O_2^- ions on the basis of the pre-edge structure in the O K-edge XAS spectrum. Croy *et al.*[40] reported molecular dynamics simulation results for the $xLi_2MnO_3\cdot(1-x)LiNi_{0.5}Mn_{0.5}O_2$ system and showed that, when Li^+ ions are removed from the system, the oxygen atoms in the Li_2MnO_3 domain are displaced from their original position and form O–O bonds with a bond length of 1.3–1.7 Å. This bond length is similar to that of the superoxide. In our study using the Li_2MnO_3 single-phase electrode, we confirmed that superoxide- and peroxide-like states

emerge after each charge process during the reversible charge/discharge cycles and that they should contribute to its increased capacity.

The O K-edge XAS structure changed throughout the potential range between 2.0 V and 4.8 V, whereas the Mn L-edge spectrum remained unchanged at potentials greater than 3.6 V. This result indicates the high degree of stability of Mn^{4+} under the strong oxidizing conditions. It further implies that O^{2-}–Mn^{4+}–O^{-} or O^{-}–Mn^{4+}–O^{-} states are more stable than the O^{2-}–$Mn^{5+/6+}$–O^{2-} state when the electrons and Li^{+} ions are extracted. Thus, from a chemical viewpoint, the oxygen radical anion $O^{\bullet -}$ will combine with a neighboring radical anion to form the peroxide ion, O_2^{2-}. The extraction of an electron from the O_2^{2-} ion should not be energetically difficult, leading to the formation of the superoxide anion O_2^{-}. In this oxygen–anion moiety of the metal complex, the O 2p orbitals are rather localized to the oxygen anions and are independent of the Mn 3d orbitals, which results in the formation of the additional O 2p bands observed in the O K-edge XAS spectrum.

Ma *et al.*[50] reported that the reversibility of the electrode reaction of Li_2MnO_3 could be improved by partially substituting Mn with Mo. In addition, the Li_2MnO_3–$LiMO_2$ (M = Ni, Co, and Mn) composite systems exhibited better cyclability compared to the Li_2MnO_3 system, which suffers from serious degradation with increasing number of cycles. The coexistence of other cation elements such as Ni and/or Co in the Li_2MnO_3–$LiMO_2$ systems appears to play an important role in maintaining the effective coordination structure for the oxygen–anion redox reactions that accompany oxygen–atom movements and/or new bond construction/destruction.[51] We are now working to elucidate the variation of the crystal structure of Li_2MnO_3 during the charge/discharge reactions, which will be discussed in a subsequent paper. This research, to elucidate the key elements that facilitate the oxygen–anion redox reactions in Li-rich layered oxide materials, is ongoing in our group.

5. Conclusions

We investigated the reversible charge compensation mechanism of an Li_2MnO_3 electrode using soft XAS analysis. We concluded that both the Mn and O ions participated in the charge compensation reactions during the reversible redox cycles. The redox reaction of Mn ions proceeded at the lower voltage of *ca.* 3.0 V *vs.* Li^{+}/Li^{0}, whereas the redox reaction of O ions proceeded throughout the voltage range between 2.0 V and 4.8 V. In the high-voltage region, electron exchange occurred mainly at the oxygen sites. The O K-edge XAS spectra showed the reversible appearance/disappearance of superoxide- and peroxide-like states during the charge/discharge reactions, suggesting the evolution/destruction of O–O bonds formed by the reorganization of oxygen networks in the electrode. These bonds contribute to the extra reversible capacity obtained in Li-rich layered manganese oxides. We presume that the Li_2MnO_3 phase in the other composite Li-rich layered electrodes contributes to the charge compensation reaction in the same manner.

Acknowledgements

The authors appreciate the experimental assistance by Mr Takahiro Kakei and Mr Yuji Kamishima, Kyoto University. This work was supported by the Research and Development Initiative for Scientific Innovation of New Generation Batteries (RISING) project from the New Energy and Industrial Technology Development Organization (NEDO) of Japan.

References

1 K. Numata, C. Sakakai and S. Yamanaka, *Solid State Ionics*, 1999, **117**, 257–263.
2 Z. Lu and J. R. Dahn, *J. Electrochem. Soc.*, 2002, **149**(7), A815–A822.
3 M. M. Thackeray, S.-H. Kang, C. S. Johnson, J. T. Vaughey, R. Benedek and S. A. Hackney, *J. Mater. Chem.*, 2007, **17**, 3112–3125.
4 T. Ohzuku, M. Nagayama, K. Tsuji and K. Ariyoshi, *J. Mater. Chem.*, 2011, **21**, 10179–10188.
5 N. Yabuuchi, K. Yoshii, S.-T. Myung, I. Nakai and S. Komaba, *J. Am. Chem. Soc.*, 2011, **133**, 4404–4419.
6 K. Mizushima, P. C. Jones, P. J. Wiseman and J. B. Goodenough, *Mater. Res. Bull.*, 1980, **15**, 783–789.
7 T. Ohzuku, A. Ueda, N. Nagayama, Y. Iwakoshi and H. Komori, *Electrochim. Acta*, 1993, **38**, 1159–1167.
8 A. R. Armstrong, M. Holzapfel, P. Novak, C. S. Johnson, S.-H. Kang, M. M. Thackeray and P. G. Bruce, *J. Am. Chem. Soc.*, 2006, **128**, 8694–8698.
9 A. Ito, Y. Sato, T. Sanada, M. Hatano, H. Horie and Y. Ohsawa, *J. Power Sources*, 2011, **196**, 6828–6834.
10 H. Koga, L. Croguennec, M. Ménétrier, P. Mannessiez, F. Weill and C. Delmas, *J. Power Sources*, 2013, **236**, 250–258.
11 M. Oishi, T. Fujimoto, Y. Takanashi, Y. Orikasa, A. Kawamura, T. Ina, H. Yamashige, D. Takamatsu, K. Sato, H. Murayama, H. Tanida, H. Arai, H. Ishii, C. Yogi, I. Watanabe, T. Ohta, A. Mineshige, Y. Uchimoto and Z. Ogumi, *J. Power Sources*, 2013, **222**, 45–51.
12 H. Koga, L. Croguennec, M. Ménétrier, K. Douhil, S. Belin, L. Bourgeois, E. Suard, F. Weill and C. Delmas, *J. Electrochem. Soc.*, 2013, **160**(6), A786–A792.
13 M. Sathiya, K. Ramesha, G. Rousse, D. Foix, D. Gonbeau, A. S. Prakash, M. L. Doublet, K. Hemalatha and J.-M. Tarascon, *Chem. Mater.*, 2013, **25**, 1121–1131.
14 M. Sathiya, G. Rousse, K. Ramesha, C. P. Laisa, H. Vezin, M. T. Sougrati, M.-L. Doublet, D. Foix, D. Gonbeau, W. Walker, A. S. Prakash, M. Ben Hassine, L. Dupont and J.-M. Tarascon, *Nat. Mater.*, 2013, **12**, 827–835.
15 M. Oishi, C. Yogi, I. Watanabe, T. Ohta, Y. Orikasa, Y. Uchimoto and Z. Ogumi, *J. Power Sources*, 2015, **276**, 89–94.
16 K. Kubobuchi, M. Mogi, H. Ikeno, I. Tanaka, H. Imai and T. Mizoguchi, *Appl. Phys. Lett.*, 2014, **104**, 053906.
17 D. Y. W. Yu, K. Yanagida, Y. Kato and H. Nakamura, *J. Electrochem. Soc.*, 2009, **156**(6), A417–A424.
18 Y. Koyama, I. Tanaka, M. Nagao and R. Kanno, *J. Power Sources*, 2009, **189**, 798–801.

19 R. Xiao, H. Li and L. Chen, *Chem. Mater.*, 2012, **24**, 4242–4251.
20 J.-M. Lim, D. Kim, Y.-G. Lim, M.-S. Park, Y.-J. Kim, M. Cho and K. Cho, *J. Mater. Chem. A*, 2015, **3**, 7066–7076.
21 S. F. Amalraj, B. Markovsky, D. Sharon, M. Talianker, E. Zinigrad, R. Persky, O. Haik, J. Grinblat, J. Lampert, M. Schulz-Dobrick, A. Garsuch, L. Burlaka and D. Aurbach, *Electrochim. Acta*, 2012, **78**, 32–39.
22 A. D. Robertson and P. G. Bruce, *Chem. Mater.*, 2003, **15**, 1984–1992.
23 Y. Paik, C. P. Grey, C. S. Johnson, J.-S. Kim and M. M. Thackeray, *Chem. Mater.*, 2002, **14**, 5109–5115.
24 N. Tran, L. Croguennec, M. Ménétrier, F. Weill, Ph. Biensan, C. Jordy and C. Delmas, *Chem. Mater.*, 2008, **20**, 4815–4825.
25 E. Lee and K. A. Persson, *Adv. Energy Mater.*, 2014, **4**, 1400498 (1–8).
26 R. Wang, X. He, L. He, F. Wang, R. Xiao, L. Gu, H. Li and L. Chen, *Adv. Energy Mater.*, 2013, **3**, 1358–1367.
27 J. Rana, M. Stan, R. Kloepsch, J. Li, G. Schumacher, E. Welter, I. Zizak, J. Banhart and M. Winter, *Adv. Energy Mater.*, 2014, **4**, 1300998 (1–12).
28 S. Han, Y. Xia, Z. Wei, B. Qiu, L. Pan, Q. Gu, Z. Liu and Z. A. Guo, *J. Mater. Chem. A*, 2015, **3**, 11930–11939.
29 W.-S. Yoon, M. Balasubramanian, K. Y. Chung, X.-Q. Yang, J. McBreen, C. P. Grey and D. A. Ficher, *J. Am. Chem. Soc.*, 2005, **127**, 17479–17487.
30 P. Strobel and B. Lambert-Andron, *J. Solid State Chem.*, 1988, **75**, 90–98.
31 A. Boulineau, L. Croguennec, C. Delmas and F. Weill, *Solid State Ionics*, 2010, **180**, 1652–1659.
32 K. Nakanishi and T. Ohta, *Advanced Topics in Measurements*, ed. Z. Zahurul Haq, InTech, Croatia, 2012, pp. 43–60.
33 A. J. Achkar, T. Z. Regier, H. Wadati, Y.-J. Kim, H. Zhang and D. G. Hawthorn, *Phys. Rev. B: Condens. Matter Mater. Phys.*, 2011, **83**, 081106 (1–4).
34 J. Stöhr, *NEXAFS Spectroscopy*, Springer, Berlin, 1992.
35 J. Zhou, X. Zhou, R. Li, X. Sun, Z. Ding, J. Cutler and T.-K. Sham, *Chem. Phys. Lett.*, 2009, **474**, 320–324.
36 J. Zhou, D. Hong, J. Wang, Y. Hu, X. Xie and H. Fang, *Phys. Chem. Chem. Phys.*, 2014, **16**, 13838–13842.
37 J. Graetz, A. Hightower, C. C. Ahn, R. Yazami, P. Rez and B. Fultz, *J. Phys. Chem. B*, 2002, **106**, 1286–1289.
38 F. M. F. de Groot, M. Grioni, J. C. Fuggle, J. Ghijsen, G. A. Sawatzky and H. Petersen, *Phys. Rev. B: Condens. Matter Mater. Phys.*, 1989, **40**, 5715–5723.
39 A. Manthiram and J. Choi, *J. Power Sources*, 2006, **159**, 249–253.
40 J. R. Croy, H. Iddir, K. Gallagher, C. S. Johnson, R. Benedek and M. Balasubramanian, *Phys. Chem. Chem. Phys.*, 2015, **17**, 24382–24391.
41 P. Rozier and J. M. Tarason, *J. Electrochem. Soc.*, 2015, **162**, A2490–A2499.
42 M. Saubanère, E. McCalla, J.-M. Tarascon and M.-L. Doublet, *Energy Environ. Sci.*, 2016, **9**, 984–991.
43 T. Ohzuku, M. Nagayama, K. Tsujia and K. Ariyoshi, *J. Mater. Chem.*, 2011, **21**, 10179–10188.
44 S. Taminato, M. Hirayama, K. Suzuki, N. L. Yamada, M. Yonemura, J. Y. Son and R. Kanno, *Chem. Commun.*, 2015, **51**, 1673–1676.
45 J.-S. Kang, D. H. Kim, J. H. Hwang, J. Baik, H. J. Shin, M. Kim, Y. H. Jeong and B. I. Min, *Phys. Rev. B: Condens. Matter Mater. Phys.*, 2010, **82**, 193102.
46 E. Yilmaz, C. Yogi, K. Yamanaka, T. Ohta and H. R. Byon, *Nano Lett.*, 2013, **13**, 4679–4684.
47 J. B. Goodenough and Y. Kim, *Chem. Mater.*, 2010, **22**, 587–603.
48 J. B. Goodenough and Y. Kim, *J. Solid State Chem.*, 2009, **182**, 2904–2911.
49 J. Rouxel, *Chem.–Eur. J.*, 1996, **2**, 1053–1059.
50 J. Ma, Y.-N. Zhou, Y. Gao, Q. Kong, Z. Wang, X.-Q. Yang and L. Chen, *Chem.–Eur. J.*, 2014, **20**, 1–9.
51 S. Hy, J.-H. Cheng, J.-Y. Liu, C.-J. Pan, J. Rick, J.-F. Lee, J.-M. Chen and B. J. Hwang, *Chem. Mater.*, 2014, **26**, 6919–6927.

